Hindawi
Mathematical Problems in Engineering
Volume 2020, Article ID 4963738, 19 pages
https://doi.org/10.1155/2020/4963738

Research Article

Research on Speed Scheme for Precise Attack of Miniature Loitering Munition

Zhidong Zhang, Jie Li, Yachao Yang, Chengwei Yang, and Ruizhi Mao

School of Mechatronical Engineering, Beijing Institute of Technology, Beijing 100081, China

Correspondence should be addressed to Chengwei Yang; yangchengwei2009@126.com

Received 10 March 2020; Revised 23 May 2020; Accepted 1 July 2020; Published 18 September 2020

Academic Editor: Marco Pizzarelli

Copyright © 2020 Zhidong Zhang et al. This is an open access article distributed under the Creative Commons Attribution License, which permits unrestricted use, distribution, and reproduction in any medium, provided the original work is properly cited.

The loitering munitions are advanced new ammunitions, which reflect both the characteristics of UAV and missile and have their own novel characteristics. This paper analysed the characteristics of the attack process of a small loitering munition and proposed a speed scheme suitable for precise strike of loitering munitions based on the concept of traditional ammunition's speed-thrust schemes. Then, the boundary conditions and the existence of the solution have been discussed. Finally, flight test results showed that the scheme was effective.

1. Introduction

A loitering munition (LM), as a new member of the precision-guided munitions [1–5], fits in the niche between cruise missiles and unmanned combat aerial vehicles (UCAVs) sharing characteristics with both. In the cruise section, the LM mainly conducts flight and mission target search in the form of a UAV, but in the launch section and the final guidance-attacking section, the LM works as a missile [5–7]. After launch, the original folded wings are unfolded, and the aircraft is converted from projectile form to drone form, and the configuration of the loitering munitions does not change again after the conversion of the machine finished [1, 8–10]. Therefore, it is a challenge for a LM to adapt to the control requirements of different mission phases under the same aerodynamic shape. The typical working process for a loitering munition includes pneumatic launch, loitering and gathering intelligence, locking on target, aborting mission, or precise attack. Some mature products of small LM are shown in Figure 1, and the working process diagram for a LM can be seen in Figure 2 [11].

Traditional precision-guided munitions include various types of guided missile, guided bomb, guided projectile, and cruise missile [2, 12–14]. The design of the propulsion system and guidance control system occupies important positions in the system design, but they are kept independent as usual. The main goal of propulsion design is to achieve effective range and reach the final flight speed to meet the requirements of the attack mission [15]. For example, the antitank missile uses a rocket engine as the propulsion to fly at high speed, and its main speed schemes include the following three types: boost + glide flight, boost + acceleration cruising + glide flight, and acceleration boost + constant velocity (boost + cruising flight). A propulsion map and speed of typical high-speed kinetic energy antitank missile are shown in Figure 3, and in general, while designing the guidance algorithms ,it will be assumed that the flight speed is constant, especially at the terminal guidance phase [16–18], or the flight speed is time varying passively affected by gravity, propulsion, and aerodynamic forces [12, 19–21]. At the same time, the research topic of speed is mainly focused on the cruise flight process [22, 23] or is considered as a terminal constraint at some special flight mission, for example, a rendezvous mission to a tanker [24].

Because the pneumatic layout and aerodynamic characteristics of LMs are closer to UAV than to missiles [25, 26], it is unreasonable to assume that the speed is constant or ignore the dynamic adjustable characteristics of speed just like a traditional precision-guided munition in designing the guidance and control algorithms in the terminal guidance

(a) (b) (c)

Figure 1: Some mature products of small LM: (a) HAROP drones, (b) Predator AX-1, and (c) Hero-900.

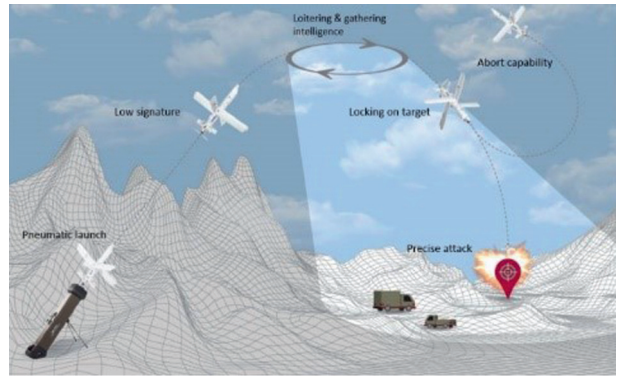

Figure 2: Working process diagram for a LM.

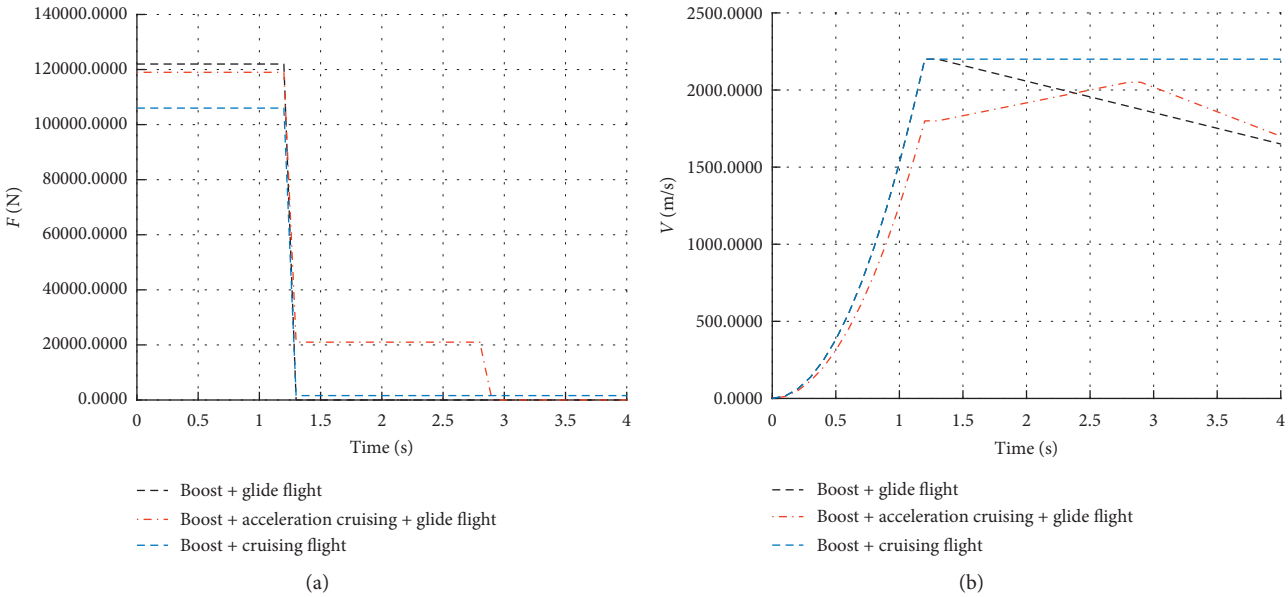

Figure 3: Propulsion map and speed of typical high-speed kinetic energy antitank missile.

phase. Therefore, it is of great significance to carry out research on the speed scheme at the terminal attack stage for a LM.

This paper is concerned with the problem of designing speed-trajectory characteristics of the LM within the attack phase. First of all, the speed requirement of guidance and control design in the LM's precision attacking process is discussed. Then, a speed scheme is proposed to improve the accuracy of a LM strike. In the following sections, the boundary condition for the establishment of the scheme is

given, and the existence conditions of the system solution is analysed. Finally, a flight test has been implemented to verify the theoretical rationality and practical value of the proposed scheme, where a method for parameter acquisition was given at the same time.

It should be noted that the main topic of this paper is to analyse the dynamic characteristics of thrust and velocity, mainly from the theoretical analysis to solve the problems in practical applications, so the specific implementation of propulsion is not discussed.

2. Speed Scheme for Miniature LM's Precision Attack

2.1. Equations of Aircraft Motion. As a novel precision-guided munition, LM in the form of small UAV could use the low-cost strap-down seeker [12, 27, 28] to achieve target capture and tracking during autonomous attack mission, so we discuss problems based on strap-down seeker against a stationary target.

The flight model was expressed by differential equations in body-fixed coordinate which was defined as follows: the origin of coordinate system is located at the LM centroid. X axis is aligned with the longitudinal axis of LM; positive direction points to the LM's nose. Y axis is perpendicular to the longitudinal axis and lies in horizontal plane; positive direction points to right. Z axis is perpendicular to XY plane; positive direction points down. This body-fixed coordinate system is illustrated in Figure 4.

In order to introduce the speed scheme clearly, only the longitudinal motion of a LM has been discussed. The force analysis of a LM is shown in Figure 5, and the homing guidance geometry of missile-target engagement of the flight process is shown in Figure 6.

L is the lift force (aerodynamic force along z direction), D is the drag force (aerodynamic force along x direction), T is the thrust of engine, m is the mass of LM, g is the gravitational acceleration, and θ is the pitch angle (Euler angle along y axis) of LM.

R is the instantaneous separation between LM and target, V is the speed of the loitering munition in x direction in body-coordinate, V_Γ is the speed of the loitering munition in z direction in body-coordinate, η is the angle made by the line of sight with respect to the fixed reference, and q is the pitch rate (angular rate along y axis).

Assume that V_Γ is small and θ is close to η, and the thrust T is assumed to act through the LM centroid and along the x axis. Then, from the engagement geometry and the force analysis of the aircraft, we can see the following.

The relative motion relationship between the LM and the target can be described as the following equations:

$$\begin{aligned} \dot{R} &= -V\cos(\theta-\eta), \\ \dot{\eta} &= -\frac{1}{R}V\sin(\theta-\eta). \end{aligned} \tag{1}$$

The dynamic equations of the LM can be written as follows:

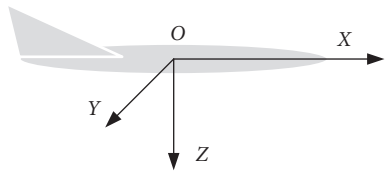

Figure 4: Body-fixed coordinate.

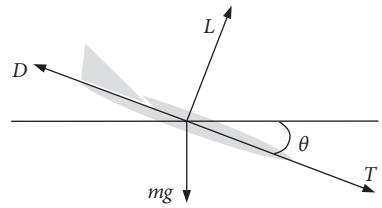

Figure 5: Force analysis of LM.

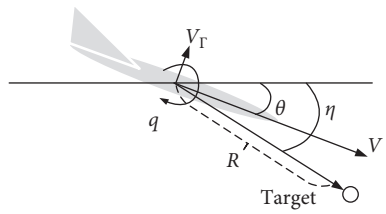

Figure 6: Two-dimensional homing guidance geometry of missile-target engagement.

$$\begin{aligned} \dot{V} &= \frac{1}{m}(T - D - mg\sin(\theta)), \\ \dot{V}_\Gamma &= \frac{1}{m}(mVq + mg\cos(\theta) - L), \\ \dot{\theta} &= q, \\ \dot{q} &= \frac{M}{I_y}, \end{aligned} \tag{2}$$

where I_y is the LM's moment of inertia in y direction.

The equations of aerodynamic force and moment can be written as follows:

$$\begin{aligned} D &= C_D QS, \\ L &= C_L QS, \\ M &= C_m QSc_A, \end{aligned} \tag{3}$$

where$M$ is the aerodynamic moment component in y direction, C_D is the drag coefficient, C_L is the lift coefficient, C_m is the pitching moment coefficient, Q is the dynamic pressure, S is the reference area, and c_A is the mean aerodynamic chord.

In the above expressions, the pitching moment coefficient can be expressed as

$$C_m = C_{mL}L + C_{m\delta_e}\delta_e + C_{mq}\left(\frac{qc_A}{2V}\right), \tag{4}$$

where C_{mL} is the moment derivative with respect to lift, $C_{m\delta_e}$ is the moment derivative with respect to control-surface deflection, δ_e is the control-surface deflection, and C_{mq} is the moment derivative with respect to pitch rate.

The dynamic pressure can be expressed as

$$Q = \frac{1}{2}\rho V^2, \tag{5}$$

where ρ is the density of air.

Then, the equations describing the LM's motion for the attacking stage can be expressed as

$$\begin{cases} \dot{R} = -V\cos(\theta - \eta), \\ \dot{\eta} = -\dfrac{1}{R}V\sin(\theta - \eta), \\ \dot{V} = \dfrac{1}{m}\left(T - \dfrac{1}{2}\rho V^2 C_D S - mg\sin(\theta)\right), \\ \dot{V}_\Gamma = \dfrac{1}{m}(mVq + mg\cos(\theta) - L), \\ \dot{\theta} = q, \\ \dot{q} = \dfrac{\left(C_{mL}((1/2)\rho V^2 C_L S) + C_{m\delta_e}\delta_e + C_{mq}\left(qc_A/2V\right)\right)(1/2)\rho V^2 S c_A}{I_y}. \end{cases} \tag{6}$$

The state variables of the system during attacking can be selected as

$$X = [R, \eta, V, V_\Gamma, \theta, q]. \tag{7}$$

The control variables are

$$U = [T, \delta_e]. \tag{8}$$

Equation (6) can be organized as

$$\begin{cases} \dot{R} = -V\cos(\theta - \eta), \\ \dot{\eta} = -\dfrac{1}{R}V\sin(\theta - \eta), \\ \dot{V} = -\dfrac{\rho C_D S}{2m}V^2 - g\sin(\theta) + \dfrac{1}{m}T, \\ \dot{V}_\Gamma = -\dfrac{\rho C_L S}{2m}V^2 + Vq + g\cos(\theta), \\ \dot{\theta} = q, \\ \dot{q} = \dfrac{C_{mL}C_L(1/4)\rho^2 S^2 c_A}{I_y}V^4 + \dfrac{C_{mq}(1/4)\rho S c_A^2}{I_y}Vq \\ \quad + \dfrac{C_{m\delta_e}(1/2)\rho S c_A}{I_y}V^2\delta_e. \end{cases} \tag{9}$$

This is the system equation that describes the motion of the aircraft at the attacking phase.

2.2. A Speed Scheme Suitable for a LM with Strap-Down Seeker for the Attacking Stage. For a LM with strap-down seeker, it is important to keep flight stabilized to get an ideal target tracking feedback, which means there should be no excessive normal shifting motion during attacking. The desired normal acceleration should be set:

$$\dot{V}_\Gamma = 0. \tag{10}$$

According to the 4th expression of equation (9), this condition can be described as

$$-\frac{\rho C_L S}{2m}V^2 + Vq + g\cos(\theta) = 0. \tag{11}$$

It can be solved from the above equation that the expected speed during the attacking process is

$$V_{tc} = \frac{mq + \sqrt{m^2q^2 + 2\rho C_L S m g\cos(\theta)}}{\rho C_L S}, \tag{12}$$

where the subscript "tc" indicates that the value of the variable is an expected value which depends on the attacking process.

When the LM is flying at this expected speed, it means

$$\dot{V} = 0. \tag{13}$$

According to the 3rd expression of equation (9), this condition can be described as

$$-\frac{\rho C_D S}{2m}V^2 - g\sin(\theta) + \frac{1}{m}T = 0. \tag{14}$$

By substituting equation (12) into equation (14), the equilibrium thrust required should be

$$T_{tc} = \frac{1}{2}\rho V_{tc}^2 C_D S + mg\sin(\theta). \tag{15}$$

A speed scheme that satisfies strap-down LM precision attack requirements could be defined by equations (14) and (15), and it can be formed as

$$\begin{cases} V_{tc} = \dfrac{mq + \sqrt{m^2q^2 + 2\rho C_L S m g\cos(\theta)}}{\rho C_L S}, \\ T_{tc} = \dfrac{1}{2}\rho V_{tc}^2 C_D S + mg\sin(\theta). \end{cases} \tag{16}$$

2.3. Analysis of the Speed Scheme's Characteristic

2.3.1. Boundary Conditions for the Solution. From equation (16), we can see that the parameters affecting the equations can be divided into two parts. We named them the static parameters and the dynamic parameters. The static parameters mainly include the gravitational acceleration, LM's weight, the density of air, and the wing reference area. The dynamic parameters mainly include lift coefficient, drag coefficient, pitch rate, and pitch angle. In this paper, the

static parameters were mainly regarded as known conditions and only the dynamic parameters have been analysed.

(1) Pitch Angle Limited Value Ensures That the Thrust Has a Solution. The solution of the speed scheme requires

$$\begin{cases} V_{\text{tc}} > 0, \\ T_{\text{tc}} \in [0, T_{\max}], \end{cases} \tag{17}$$

where $T_{\max}$ is the maximum thrust of the engine.

It can be seen from equation (16) that $V_{\text{tc}} > 0$ is obvious; for T_{tc}, there is

$$0 \le \frac{1}{2}\rho V_{tc}^2 C_D S + mg\sin(\theta) \le T_{\max}. \tag{18}$$

The design of the propulsion system should naturally meet the upper boundary requirements, so this paper studied the lower boundary of the pitch angle only.

According to (18), when given a certain drag coefficient, there is

$$\theta \ge \arcsin\left(-\frac{(1/2)\rho V_{tc}^2 C_D S}{mg}\right), \quad \theta \in \left[-\frac{\pi}{2}, 0\right]. \tag{19}$$

That means

$$\theta_{lb} = \arcsin\left(-\frac{(1/2)\rho V_{tc}^2 C_D S}{mg}\right), \tag{20}$$

where the subscript "*lb*" means this pitch angle is the lower boundary for speed scheme to have a positive thrust.

Therefore, in order to meet the requirements of this scheme, the relationship between the limit value of the pitch angle and the flight speed during the attacking must obey the expression above, and it can be represented by a curve, as shown in Figure 7:

According to equation (20), for different LMs or just for different flight status, if the drag coefficient CD is changing, the above curve in Figure 7 should be turned to a surface, which satisfies the relationship between the pitch angle value and the drag coefficient CD, as shown in Figure 8.

It can be seen from Figure 8 that while the speed is constant, the greater the drag coefficient the steeper the pitch angle, and while the drag coefficient is constant, the greater the speed the steeper the pitch angle.

(2) Balance between Flight Speed and Pitch Angle. While the LM's lift coefficient is constant, it can be seen from the scheme equation (16) that the larger the pitch angle (absolute value) is, the smaller the flight speed that satisfies the normal equilibrium condition. According to the 1st expression of equation (16), a balance pitch can be calculated by equation (21), and the balance map of flight speed and pitch angle is shown in Figure 9.

$$\theta_{\text{balance}} = \operatorname{acrcos}\left(\frac{V_{tc}^2 \rho C_L S - 2V_{tc} mq}{2mg}\right), \tag{21}$$

where the subscript "balance" means this value is specific for the variable (pitch angle) to meet the speed scheme's expected speed V_{tc}.

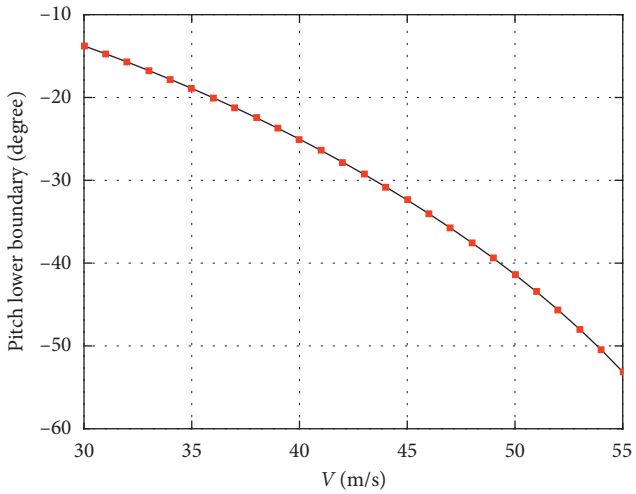

Figure 7: Lower boundary map of pitch angle according to the speed scheme. Different speeds give different lower boundaries for the pitch angle.

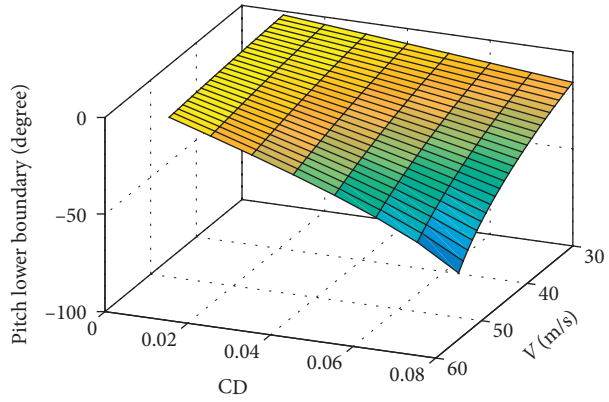

Figure 8: Lower boundary map of pitch angle according to different CD.

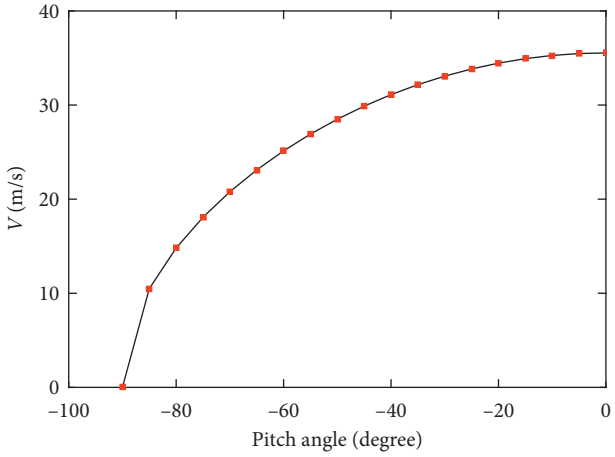

Figure 9: Balance map of flight speed and pitch angle.

In addition, when CL changes within a certain range with flight conditions, the relationship between balance pitch angle, CL, and speed is shown in Figure 10:

As can be seen from the above figure, in order to obtain a large attacking speed and obtain a steep attacking angle, the LM should have a small lift coefficient.

(3) *Valid Pitch Angles according to Prerequisites of Lower Boundary and the Balance Relationship*. For a given set of aerodynamic characteristics [CD, CL], it can be known from the speed scheme that the pitch angle during attacking must satisfy both the lower boundary and the balance relationship we have given. We named these pitch angles "valid pitch angles." This requirement is described in Figure 11.

When the aerodynamic characteristics [CD, CL] change within a certain range, valid pitch angles that satisfy the solution of the speed scheme under different conditions can be obtained, as shown in Figure 12.

Therefore, the valid pitch angles during attacking phase with respect to certain aerodynamic parameters can be expressed as

$$\theta_{\text{valid}} \in \left\{\theta \geq \theta_{\text{lb}} \,\middle|\, \theta = \theta_{\text{blance}}\right\}, \tag{22}$$

where the subscript "valid" means the pitch angle satisfies both the lower boundary and the balance relationship.

According to equation (22), if the lift coefficient and the drag coefficient of a LM during attacking are known, we can calculate the boundary condition and the balance points of the pitch angle and then set the attack conditions according to a valid pitch angle. At the same time, the thrust needed can be calculated according to the speed scheme.

2.3.2. The Existence and Uniqueness of Solution to the Motion of the LM. Having determined the boundary conditions of the solution, we only know that the scheme has the application basis with the corresponding conditions. In this section, the LM's motion reliability during the attacking flight was confirmed. We attributed this problem to a uniqueness problem of the system solution [29].

When the design of the control system is completed, the ideal attitude control loop can be equivalent to an inertia unit with a time constant of T_θ. Assume that the flight process is stable and the guidance process is implemented by the tracking guidance law, that is, the pitch rate is 0 ($q \approx 0$). Combine the proposed speed scheme equation (16) with the LM motion equation (9), and a new description of the system can be given:

$$\begin{cases} \dot{R} = -V\cos(\theta - \eta), \\ \dot{\eta} = -\dfrac{1}{R}V\sin(\theta - \eta), \\ \dot{V} = \dfrac{\rho C_D S}{2m}\left(\left(\dfrac{\sqrt{2\rho C_L S m g\cos(\theta)}}{\rho C_L S}\right)^2 - V^2\right), \\ \dot{V}_\Gamma = -\dfrac{\rho C_L S}{2m}V^2 + g\cos(\theta), \\ \dot{\theta} = \dfrac{\eta - \theta}{T_\theta}. \end{cases} \tag{23}$$

System (23) can be linearized at any working point and expressed as follows:

$$\dot{x}(t) = Ax. \tag{24}$$

Based on Taylor's expansion, the system characteristic matrix can be given as follows:

$$A = \begin{bmatrix} 0 & -V_e\sin(\theta_e - \eta_e) & -\cos(\theta_e - \eta_e) & 0 & V_e\sin(\theta_e - \eta_e) \\ \dfrac{V_e}{R_e^2}\sin(\theta_e - \eta_e) & \dfrac{V_e}{R_e}\cos(\theta_e - \eta_e) & \dfrac{-1}{R_e}\sin(\theta_e - \eta_e) & 0 & \dfrac{-V_e}{R_e}\cos(\theta_e - \eta_e) \\ 0 & 0 & \dfrac{-\rho C_D S V_e}{m} & 0 & -\dfrac{C_L}{C_D g}\sin\theta_e \\ 0 & 0 & \dfrac{-\rho C_L S V_e}{m} & 0 & -g\sin\theta_e \\ 0 & \dfrac{1}{T_\theta} & 0 & 0 & \dfrac{-1}{T_\theta} \end{bmatrix}. \tag{25}$$

The index of the variable "e" identifies the value at the working point, for example, flying according to the speed scheme is a special case.

It can be seen from the system characteristic matrix that the elements in the fourth column are all zero. That means the normal velocity V_Γ does not affect the condition of the

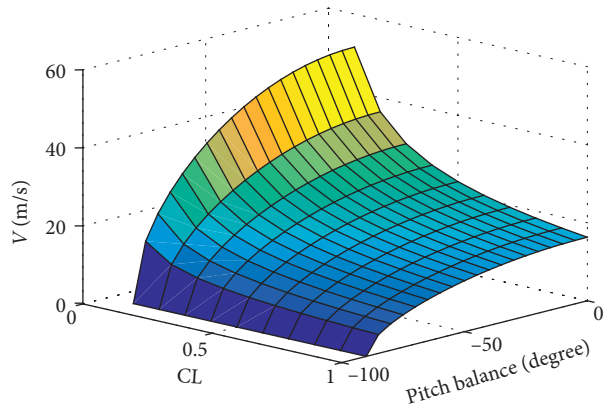

Figure 10: Balance map of pitch angle, flight speed, and CL.

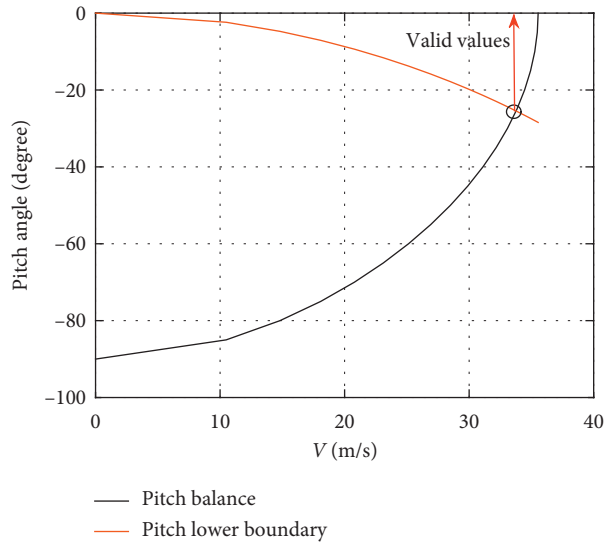

Figure 11: Valid pitch angle map according to both lower boundary and the balance relationship.

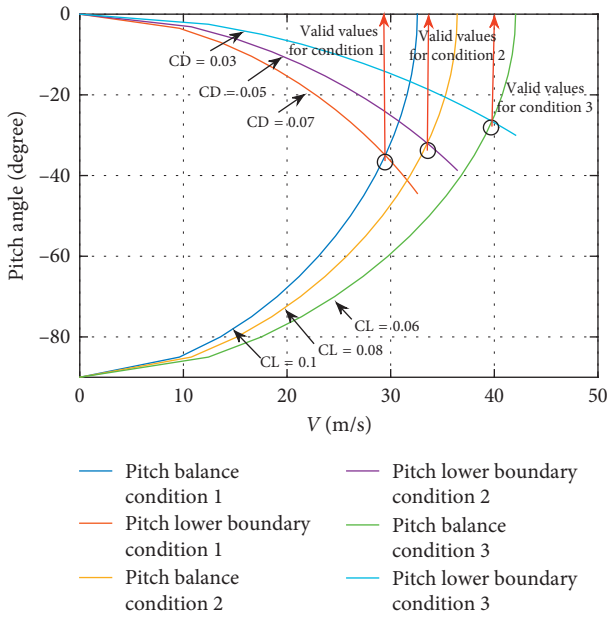

Figure 12: Valid pitch angle map with different aerodynamic conditions: condition 1: CL = 0.1, CD = 0.07; condition 2: CL = 0.08, CD = 0.05; condition 3: CL = 0.06, CD = 0.03.

system. So, in order to simplify the analysis of the system, the influence of the normal velocity can be ignored, and a simplified system characteristic matrix can be given:

$$A^* = \begin{bmatrix} 0 & -V_e \sin(\theta_e - \eta_e) & -\cos(\theta_e - \eta_e) & V_e \sin(\theta_e - \eta_e) \\ \frac{V_e}{R_e^2} \sin(\theta_e - \eta_e) & \frac{V_e}{R_e} \cos(\theta_e - \eta_e) & \frac{-1}{R_e} \sin(\theta_e - \eta_e) & \frac{-V_e}{R_e} \cos(\theta_e - \eta_e) \\ 0 & 0 & \frac{-\rho C_D S V_e}{m} & -\frac{C_L}{C_D g} \sin\theta_e \\ 0 & \frac{1}{T_\theta} & 0 & \frac{-1}{T_\theta} \end{bmatrix}. \tag{26}$$

So, we get

$$\left|A^*\right| = \frac{C_L V_e}{C_D g T_\theta R_e^2} \sin\theta_e \sin(\theta_e - \eta_e) \cos(\theta_e - \eta_e). \tag{27}$$

According to the compression mapping principle [30], when the system parameters meet the condition

$$\left|A^*\right| < 1, \tag{28}$$

the system should have a unique solution.

3. Scheme Verification

After analysing the boundary conditions and the uniqueness of the solution, requirements of the program application have been grasped basically. So, we carry out the verification work next.

First of all, the steps of the test were introduced. In this work, we found that there were many different methods to obtain the parameters the test needs, and different methods are different in difficulty and accuracy. Therefore, a method to get the lift coefficient and drag coefficient was introduced first, and then the experimental flow of scheme verification was given.

3.1. Acquisition of Parameters and the Scheme Testing Process. The thrust was calculated according to the equation (16), wherein the LM weight m, the density of air, the wing reference area, and the gravitational acceleration can be regarded as known parameters. The pitch angle and the pitch rate could be measured with sensors during the flight. Therefore, the lift coefficient and the drag coefficient were the key parameters for the realization of the speed and thrust scheme, which needs to be acquired for the verification of flight test. The following is a further explanation of the acquisition of the lift coefficient and the drag coefficient before the verification process.

For small-sized aircraft, obtaining aerodynamics data through wind tunnel test has the disadvantages of complicated experiment and high cost. Especially for occasions requiring rapid prototyping and special control performance verification, traditional wind tunnel test cannot meet low cost and rapid evaluation in engineering application.

The commonly used methods also include the aerodynamic parameter identification method based on flight test and the means of simulation calculation [31–34]. The main disadvantage of the simulation calculation is that the accuracy cannot be reliably guaranteed, and the result needs to be evaluated and revised using a series of experimental data.

In order to reduce the cost of experiments and quickly obtain parameters closer to the actual situation than simulation calculations and in order to ensure the safety of the test, this paper adopted the aerodynamic parameter identification method of the aircraft balance point based on an object understanding calculation method.

According to equation (9), the formulas we introduced to calculate the lift coefficient and the drag coefficient are

$$C_L = \frac{V_{\text{fly\_data}} q_{\text{fly\_data}} - \dot{V}_{\Gamma\text{fly\_data}} + g\cos\theta_{\text{fly\_data}}}{(1/2)\rho V_{\text{fly\_data}}^2 (S/m)},$$
$$C_D = \frac{T_{\text{fly\_data}} - \dot{V}_{\text{fly\_data}} - mg\sin\theta_{\text{fly\_data}}}{(1/2)\rho V_{\text{fly\_data}}^2 S}, \tag{29}$$

where the subscript "fly_data" indicates that the specific values should be obtained from a fly test.

In order to avoid the situation that the singular matrix cannot be solved and in order to obtain a more accurate solution using experimental data with measurement errors, the above equations were extended to overdetermined equations.

Rewrite the above expressions as

$$A_{\text{CL}} X_{\text{CL}} = b_{\text{CL}}, \tag{30}$$

$$A_{\text{CD}} X_{\text{CD}} = b_{\text{CD}}, \tag{31}$$

where

$$A_{\mathrm{CL}} = \begin{bmatrix} \frac{\rho S}{2m} V_{\mathrm{fly\_data}}^2(1) \\ \frac{\rho S}{2m} V_{\mathrm{fly\_data}}^2(2) \\ \cdots \\ \frac{\rho S}{2m} V_{\mathrm{fly\_data}}^2(i) \end{bmatrix}, \tag{32}$$

$$X_{\mathrm{CL}} = C_L, \tag{33}$$

$$b_{\mathrm{CL}} = \begin{bmatrix} V_{\mathrm{fly\_data}}(1) q_{\mathrm{fly\_data}}(1) - \dot{V}_{\Gamma \mathrm{fly\_data}}(1) + g\cos\theta_{\mathrm{fly\_data}}(1) \\ V_{\mathrm{fly\_data}}(2) q_{\mathrm{fly\_data}}(2) - \dot{V}_{\Gamma \mathrm{fly\_data}}(2) + g\cos\theta_{\mathrm{fly\_data}}(2) \\ \cdots \\ V_{\mathrm{fly\_data}}(i) q_{\mathrm{fly\_data}}(i) - \dot{V}_{\Gamma \mathrm{fly\_data}}(i) + g\cos\theta_{\mathrm{fly\_data}}(i) \end{bmatrix}, \tag{34}$$

$$A_{\mathrm{CD}} = \begin{bmatrix} \frac{\rho S}{2} V_{\mathrm{fly\_data}}^2(1) \\ \frac{\rho S}{2} V_{\mathrm{fly\_data}}^2(2) \\ \cdots \\ \frac{\rho S}{2} V_{\mathrm{fly\_data}}^2(i) \end{bmatrix}, \tag{35}$$

$$X_{\mathrm{CD}} = C_D, \tag{36}$$

$$b_{\mathrm{CD}} = \begin{bmatrix} T_{\mathrm{fly\_data}}(1) - \dot{V}_{\mathrm{fly\_data}}(1) - mg\sin\left(\theta_{\mathrm{fly\_data}}(1)\right) \\ T_{\mathrm{fly\_data}}(2) - \dot{V}_{\mathrm{fly\_data}}(2) - mg\sin\left(\theta_{\mathrm{fly\_data}}(2)\right) \\ \cdots \\ T_{\mathrm{fly\_data}}(i) - \dot{V}_{\mathrm{fly\_data}}(i) - mg\sin\left(\theta_{\mathrm{fly\_data}}(i)\right) \end{bmatrix}. \tag{37}$$

In the above expressions, "i" is the number of equations in the overdetermined equations. Because solving the overdetermined equation is not the focus of this article, it will not be described in detail [35, 36].

The parameter calculation and scheme test flow are given in Figure 13:

The following is a detailed description of the verification flight test process.

3.2. Prophase Flight Test for Data Collection. The prophase flight test was designed to collect data for parameter calculations. The UAV used for flight test is shown in Figure 14, and the parameters of the UAV are shown in Table 1.

A simple data acquisition and flight control module was designed. The hardware system is shown in Figures 15 and 16, and the device list is shown in Table 2.

According to the equations (32), (34), (35), and (37), the data needed to be collected include speed, pitch angle, thrust of the engine (in the experiment, the output percentage of the engine controller was collected and then converted into the actual thrust), pitch rate, and accelerations in x direction and z direction in body-coordinate frame. The data storage frequency was 50 Hz and the duration was 2 s.

The obtained experimental data are shown in the following figures: Figure 17 shows the output percentage of the engine controller, Figure 18 shows the acceleration in z direction in body-coordinate, Figure 19 shows the acceleration in x direction in body-coordinate, Figure 20 shows the pitch rate, Figure 21 shows the pitch angle, and Figure 22 shows the flight speed.

3.3. Calculation of Lift and Drag Coefficients. The lift coefficient and the drag coefficient were calculated according to equations (30) and (31) after the experimental data were obtained, and the calculation results are shown in Table 3.

3.4. Boundary Condition Calculation. According to equations (20)–(22) and the results of the previous section (see Table 3), the valid pitch angles could be calculated. The valid pitch angle map and the critical point of the valid pitch angle can be seen in Figure 23.

It can be seen that when the pitch angle is in the range of $\theta_{\mathrm{valid}} \in [-25^\circ, 0]$, there will be a valid solution of the system according to the scheme proposed in this paper, and the attacking mission could be performed.

According to the previous flight test experience, the target attack range was 100–150 m after the target was clear in the field of view limited by the camera performance (the relationship between flight altitude, camera performance, and pitch angle is complex and is not the focus of this article, so it will not be described in detail). So, the reasonable range of attack altitude should be controlled within the following range:

$$h_{\mathrm{attack}} \in \left\{ h \mid \left(\min\left(L_{\mathrm{attack}}\right) \left| \tan\left(\min\left(\theta_{\mathrm{valid}}\right)\right) \right| \right) < h < \max\left(L_{\mathrm{attack}}\right) \left| \tan\left(\min\left(\theta_{\mathrm{valid}}\right)\right) \right| \right\}, \tag{38}$$

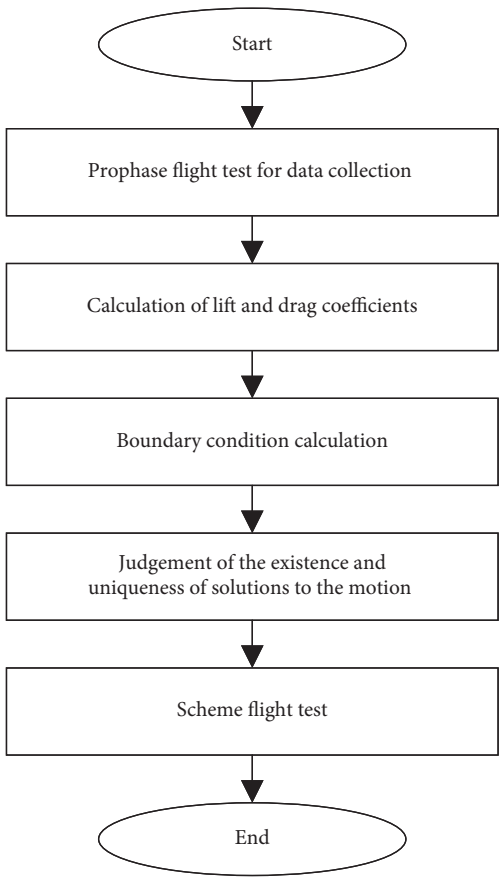

Figure 13: Flowchart of scheme test.

Figure 14: The UAV used for flight test.

Table 1: Parameters of the UAV.

Wing reference area (m^2)	Wing span (m)	Weight (kg)	Length (m)
0.46	1.2	3.5	1

where the subscript "attack" means the value is at the time the attack started.

That is,

$$h_{\text{attack}} \in \{h \mid 46.63 < h < 69.94\}. \tag{39}$$

3.5. Judgement of the Existence and Uniqueness of Solutions to the Motion. According to the experimental data analysis, the valid pitch angle was in the range of $\theta_{\text{valid}} \in [-25^{\circ}, 0]$, the flight speed was in the range of $V \in [0, 23]$, and the pitch angle response time was $T_\theta = 0.2$ s. According to equation (27),

$$\begin{aligned} \left|A^*\right| &= \frac{C_L V_e}{C_D g T_\theta R_e^2} \sin\theta_e \sin\left(\theta_e - \eta_e\right)\cos\left(\theta_e - \eta_e\right) \\ &< \frac{C_L \max(V)}{2C_D g T_\theta R_e^2} \left|\sin\left(\min\left(\theta_{\text{valid}}\right)\right)\sin\left(2\left(\theta_e - \eta_e\right)\right)\right| \\ &< \frac{C_L \max(V)}{2C_D g T_\theta R_e^2} \left|\sin\left(\min\left(\theta_{\text{valid}}\right)\right)\right|. \end{aligned} \tag{40}$$

So, the system will have a unique solution when

$$\frac{C_L \max(V)}{2C_D g T_\theta R_e^2} \left|\sin\left(\min\left(\theta_{\text{valid}}\right)\right)\right| < 1. \tag{41}$$

That is,

$$R_e > 2.2819. \tag{42}$$

It can be seen from the above calculation result that there would be a unique state trajectory in the attacking process before the distance to the target is less than 2.2819 meters. This limit distance satisfied the conditions of the test; in other words, the speed scheme proposed in this paper was feasible.

3.6. Scheme Flight Test

3.6.1. Control System Block Build according to the Speed Scheme. The logic of the flight test: use the scheme to calculate an expected thrust during the attacking phase and cooperate with the attitude control module to complete the impact task against a nonmoving target.

The control system constructed in this paper consisted of an attitude control module and a speed control module. The attitude control module was realized by a classical PID controller. The speed control module was formed according to the speed scheme. The system block diagram is shown in Figure 24.

The speed controller parameters were calculated according to equation (16) and are shown in Table 4.

3.6.2. Test Implementation Method. The UAV was the same one used in data acquisition (see Figure 14), and the flight process can be seen in Figure 25 and can be described as follows:

(1) *Take Off*. The UAV takes off by remote controller and flies to the vicinity of the target.

(2) *Regulate*. Switch the control mode to the automatic driving by the remote controller and the UAV would adjust the route and attitude automatically.

(3) *Attack*. When the target enters the field of view, it can be selected on the video; at the same time, the

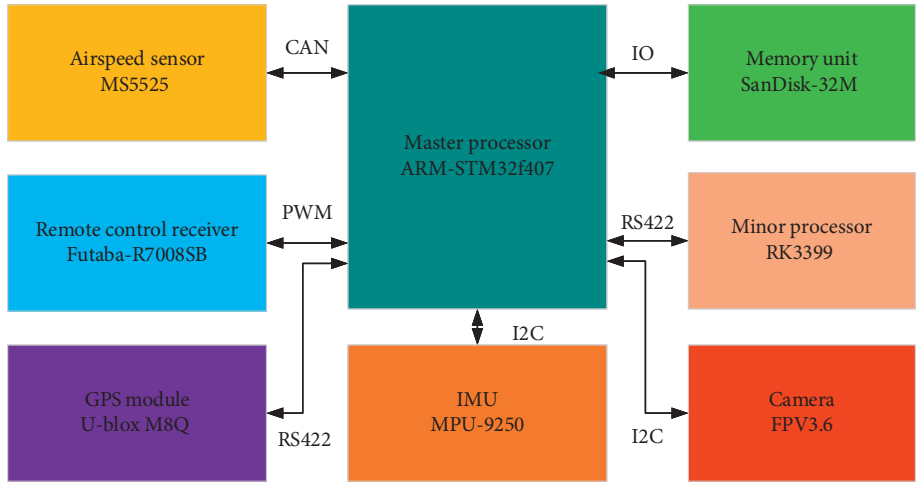

Figure 15: Hardware design structure diagram.

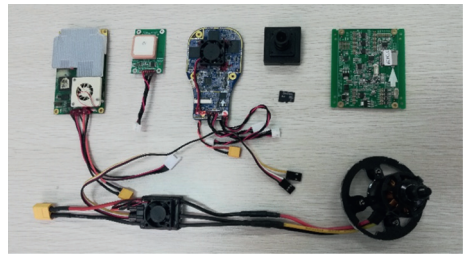

Figure 16: The experimental equipment.

Table 2: Main device list.

Module	Main device	Use of this module
Master processor	STM32F407	Airspeed calculation and flight control
Airspeed sensor	MS5525	Dynamic pressure measurement
Remote control receiver	Futaba-R7008SB	Accepting operator's remote command
GPS module	U-blox M8Q	Measuring aircraft position
IMU	MPU-9250	Measuring the inertia of the aircraft
Memory unit	SanDisk-32M	Storing experimental data in flight
Minor processor	RK3399	Image compression
Camera	FPV3.6	Video capture

controller designed in this paper starts working automatically until the UAV hits the target.

3.6.3. Flight Test Result. In this section, the result of the flight test is presented. The final 7 s flight path was selected for presentation purposes during attacking stages of the flight test, and the data are shown in the following figures: Figure 26 shows the thrust, Figure 27 shows the speed, Figure 28 shows the pitch angle, Figure 29 shows the acceleration in z direction in body-coordinate, Figure 30 shows the flight path, Figure 31 shows the first perspective video screenshot, and Figure 32 shows the third perspective video screenshot.

Based on the experimental results, following conclusions can be given:

First of all, Figures 26 and 27 show that the thrust and speed were dynamic curves, which were very different from the traditional ammunition speed throttle scheme (as can been seen in Figure 3), and their changes were all within reasonable ranges.

Secondly, as can been seen in Table 5, the mean of acceleration in z direction from the scheme flight test was -0.6351 and that from remote control test was -9.323. The standard deviation of acceleration in z direction from the scheme flight test was 1.0596 and that from remote control test was 1.727. Compared with data from the remote control test (which has been shown in Figure 18), acceleration in z direction in body frame has been suppressed clearly (as can been seen in Figure 28).

At the same time, the pitch angle and the flight trajectory curve is smooth (as shown in Figures 29 and 30), which

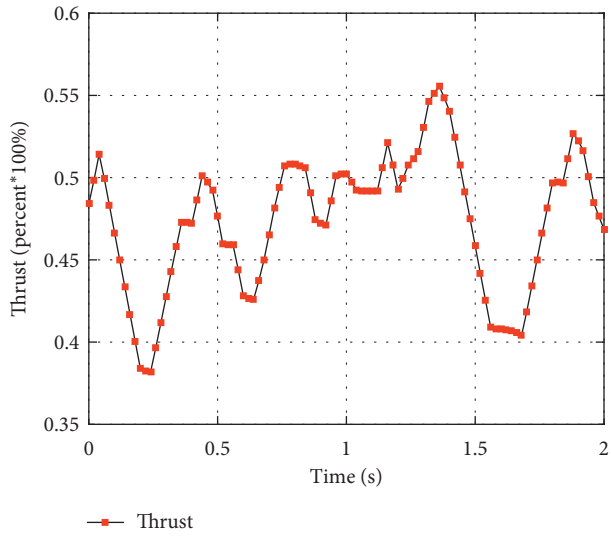

Figure 17: Output percentage of the engine controller.

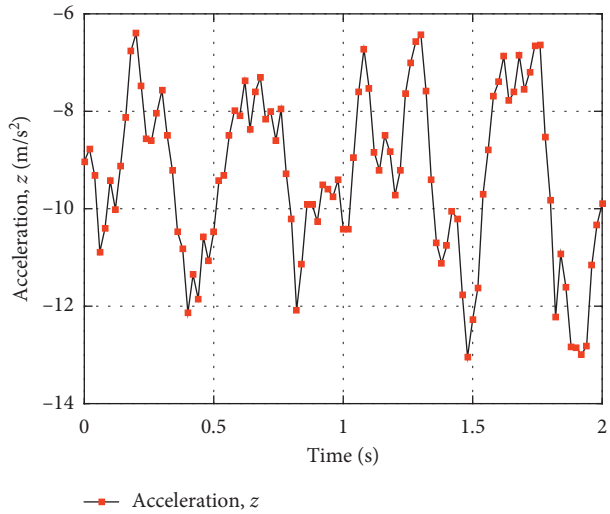

Figure 18: Acceleration in z direction in body-coordinate.

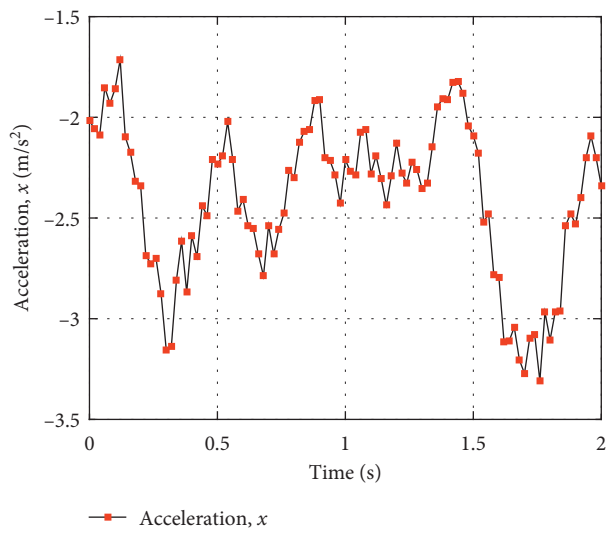

Figure 19: Acceleration in x direction in body-coordinate.

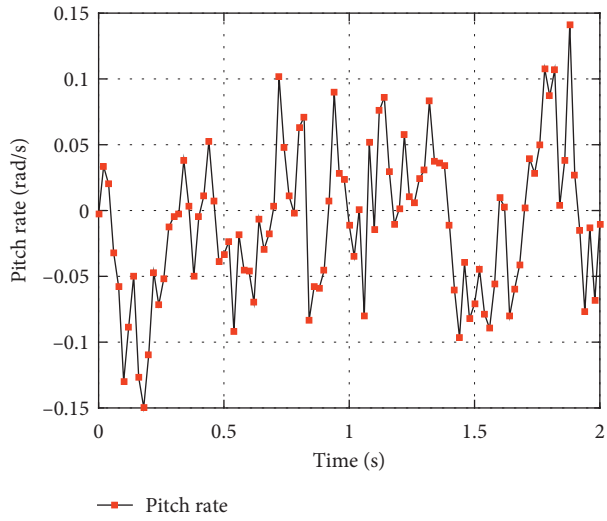

Figure 20: Pitch rate.

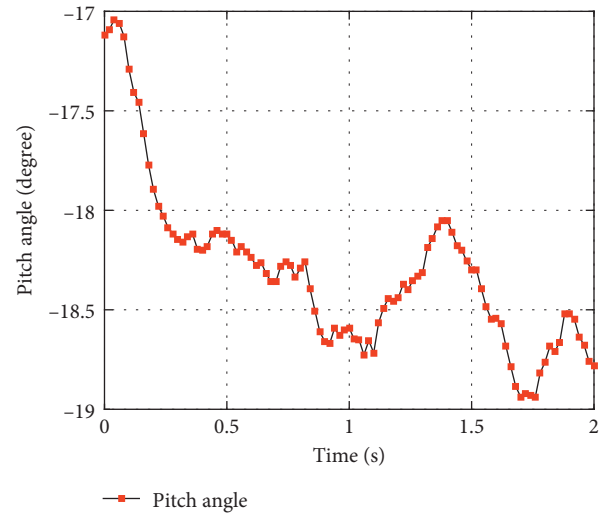

Figure 21: Pitch angle.

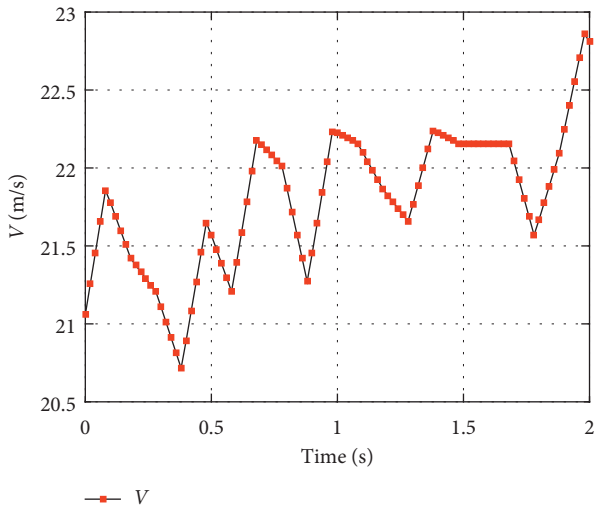

Figure 22: Speed.

Table 3: Calculation result of the lift coefficient and the drag coefficient.

Parameter	Value
CL	0.21
CD	0.1

strongly verifies that the speed scheme proposed in this paper was helpful to improve the attitude and trajectory stability of the UAV during attacking.

Finally, as can been seen in the screenshots of the flight videos (Figures 31 and 32), the UAV successfully hit the target, which further illustrated the effectiveness of the scheme.

3.6.4. Defect Analysis. However, the airspeed during the flight did not follow the expected trajectory perfectly, as shown in Figure 33. Further analysis is given below.

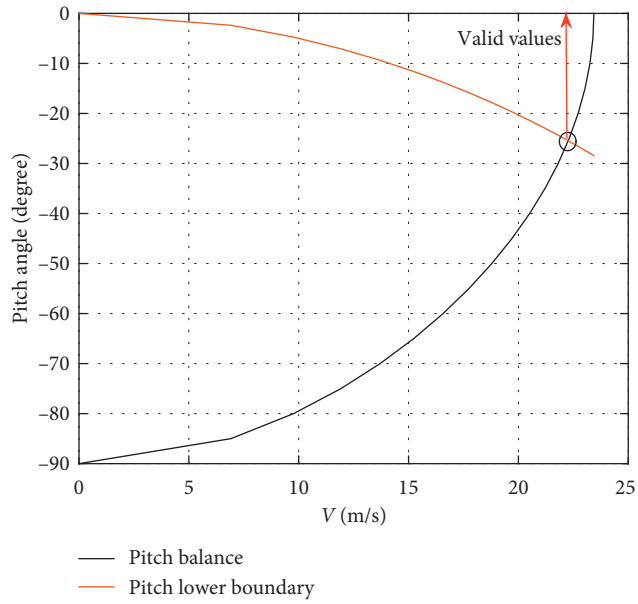

Figure 23: Valid pitch angle map established by flight test data.

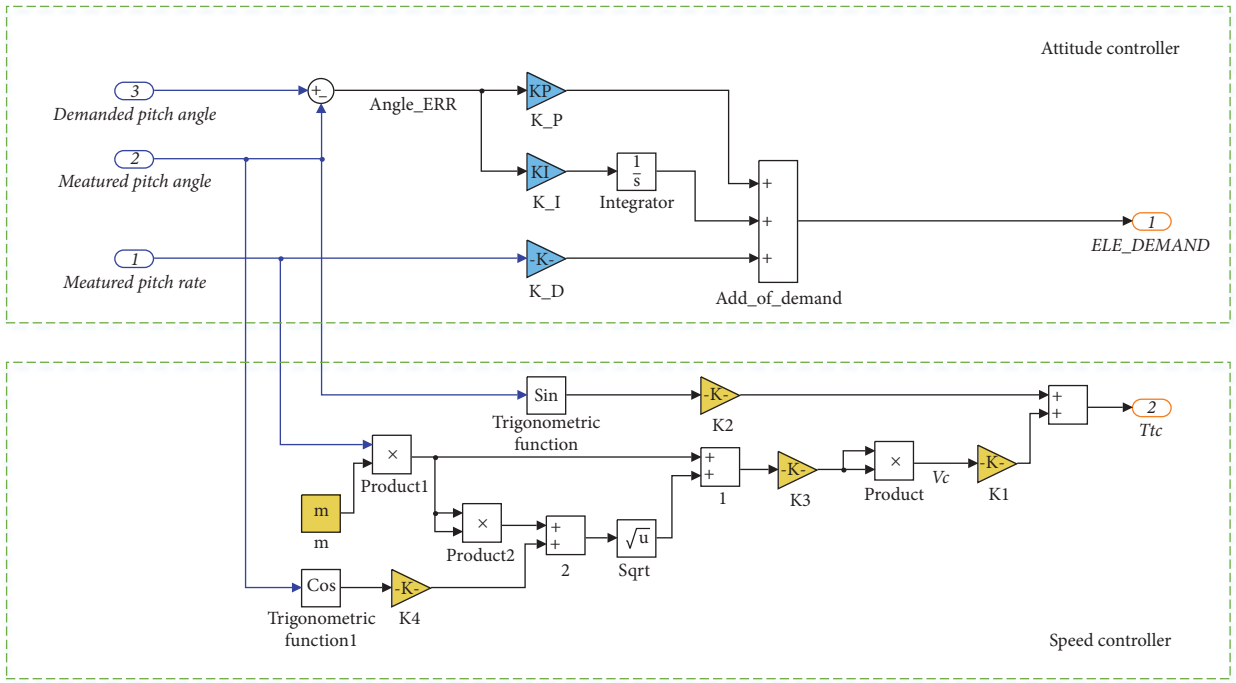

Figure 24: Control system block diagram.

(1) Dynamic Response Characteristics of the Throttle. Since the airspeed did not change much during the whole flight process, it can be assumed that the thrust depended only on the working state of the propulsion system and was independent of the atmospheric conditions. According to equation (9), using the thrust as input,

Table 4: Speed controller parameters corresponding to the scheme.

Parameter	Value
K1	0.03
K2	34.30
K3	8.01
K4	8.57

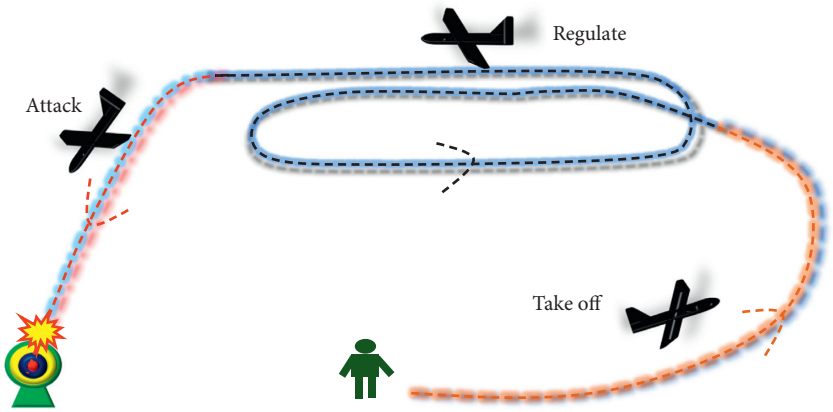

Figure 25: Flight phase diagram.

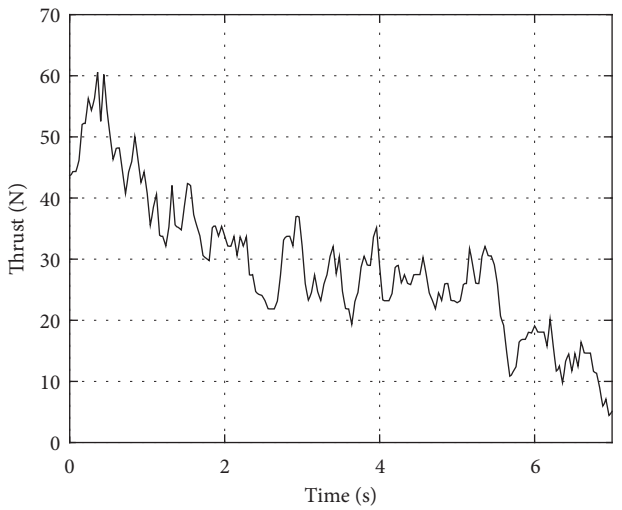

Figure 26: Thrust in flight test.

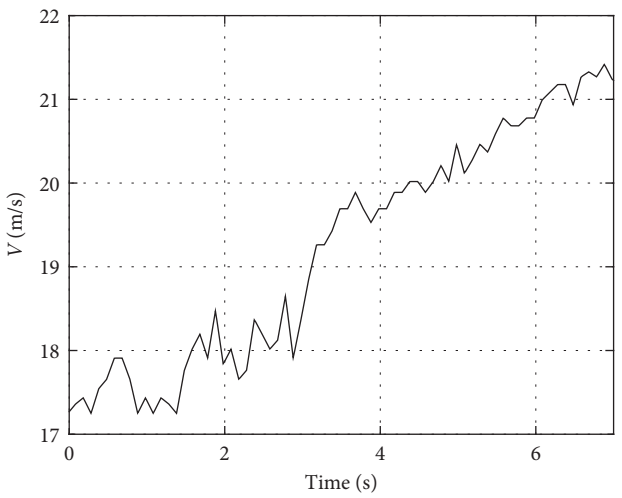

Figure 27: Speed in flight test.

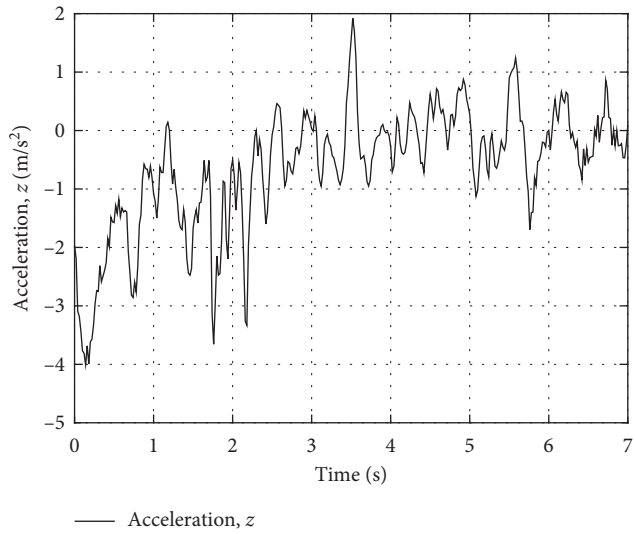

Figure 28: Acceleration in z direction in body-coordinate.

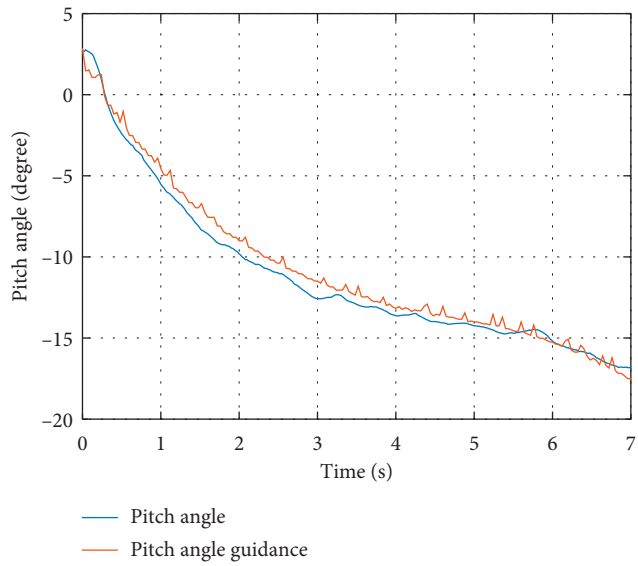

Figure 29: Pitch angle in flight test.

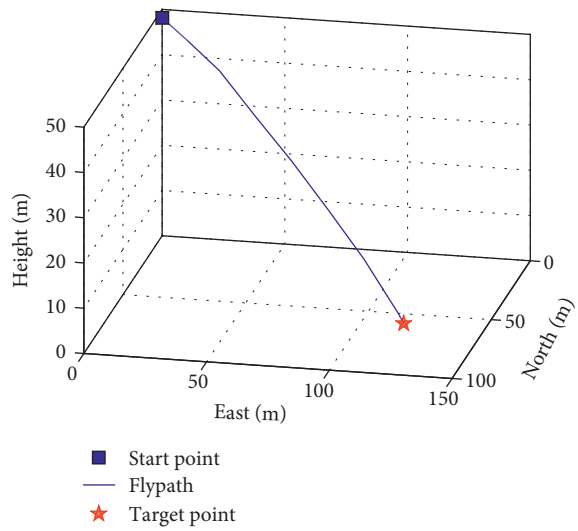

Figure 30: Flight path in flight test.

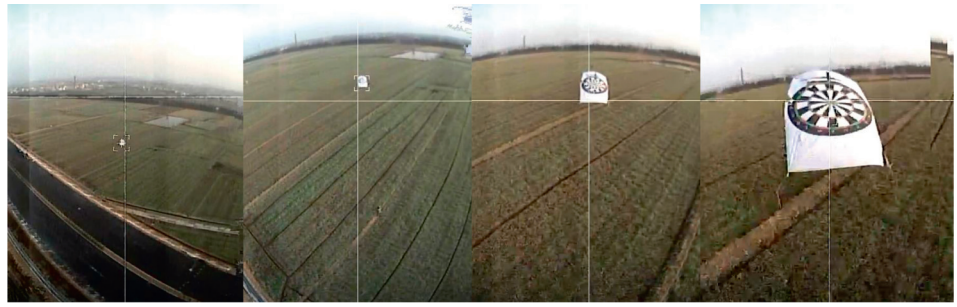

Figure 31: First perspective video screenshot in flight test.

Figure 32: Third perspective video screenshot in flight test.

Table 5: Mean and standard deviation of flight tests.

Data source	Mean	Standard deviation
Remote control test	−9.323	1.727
Scheme flight test	−0.6351	1.0596

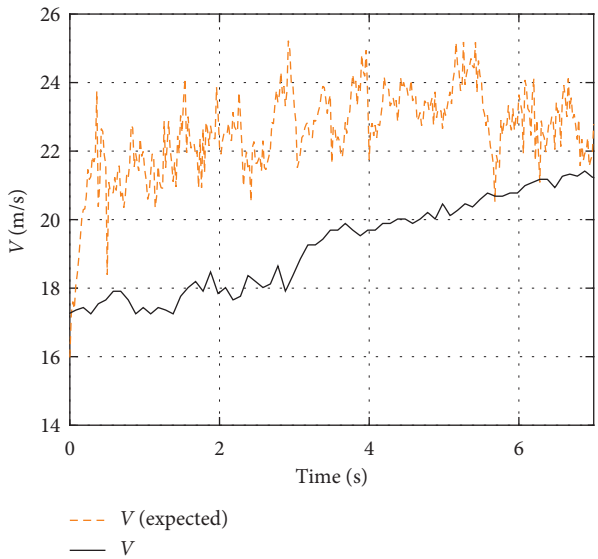

Figure 33: Tracking effect of airspeed command in automatic attack. The expected one was calculated according to equation (16).

the transfer function of the speed output can be expressed as

$$\frac{\Delta V}{\Delta T} = \frac{k_T s}{s^2 - 2\xi\omega_T s + \omega_T^2}. \tag{43}$$

Assuming that the throttle thrust input signal is step-signal $\Delta T1(t)$, based on final value theorem of Laplace transform, the speed response is

$$\Delta V(t \longrightarrow \infty) = \lim_{s \longrightarrow 0} s \bullet \left(\frac{k_T s}{s^2 - 2\xi\omega_T s + \omega_T^2} \right) \bullet \frac{\Delta T}{s} = 0. \tag{44}$$

This shows that the change of the throttle can only adjust the speed during the transition process but cannot fully achieve the purpose of controlling the speed according to the ideal trajectory.

(2) Stability Analysis of Speed. From equation (24) and the system characteristic matrix equation (25), the differential expression describing the airspeed motion process at any operating point after linearization can be given by

$$\dot{V} = \frac{-\rho C_D S V_e}{m} V - \frac{C_L}{C_D g} \sin\theta_e \theta. \tag{45}$$

When the system is aiming at the target, there is

$$\dot{V} + \frac{\rho C_D S V_e}{m} V + \frac{C_L}{C_D g} \sin\theta_e \theta_e = 0. \tag{46}$$

Its characteristic roots are

$$\zeta_{1,2} = \frac{-(\rho C_D S V_e / m) \pm \sqrt{(\rho C_D S V_e / m)^2 - 4 (C_L / C_D g) \sin\theta_e \theta_e}}{2}, \tag{47}$$

where

$$\begin{cases} \dfrac{\rho C_D S V_e}{m} > 0, \\ \dfrac{C_L}{C_D g} \sin\theta_e \theta_e > 0. \end{cases} \tag{48}$$

This means the two eigenvalues of the differential equation have negative real parts, so the change of the airspeed trajectory should satisfy the stability condition, and

the test data also illustrated this feature: the speed curve rises following the expected one (Figure 33).

However, as shown in Figure 23 (the control system block diagram), only an open-loop controller was used to control the speed to achieve the desired value V_{tc}. Obviously, an open-loop controller's performance cannot meet the requirement of a complex testing environment, and the experimental results also verified this conclusion: the speed curve rises but slowly.

It would be nice to design a better controller to improve the response characteristics of the speed, but how to improve the control law requires further analysis, and it is out of range of this research, so it is one of the tasks we will continue to expand in the future.

4. Conclusions

In this paper, a speed scheme for small loitering munitions has been given for precision strike mission. The pitch angle boundary of the solution during attack was given, and the existence and unique conditions of the system solution were analysed. Then, a flight test was taken to verify the scheme, and the result showed that the scheme was effective. At last, based on the analysis of experimental data, this paper summarizes the shortcomings of the program and proposes a clear direction for further research.

Abbreviations

L: Lift force, N
D: Drag force, N
θ: Pitch angle, rad
T: Thrust, N
m: Mass of the loitering munition, kg
g: Gravitational acceleration, m/s^2
q: Pitch rate, rad/s
η: The angle made by the line of sight with respect to the fixed reference, rad
V: The speed of the loitering munition in x direction in body-coordinate, m/s
R: The instantaneous separation between LM and target, m
V_Γ: The speed of the loitering munition in z direction in body-coordinate, m/s
I_y: The LM's moment of inertia in y direction, kg·m^2
M: Aerodynamic moment component in y direction in fixed plane coordinate, Nm
C_D: Drag coefficient
Q: Dynamic pressure, Pa
S: Reference area, m^2
C_L: Lift coefficient
C_m: (Pitching) moment coefficient
c_A: Mean aerodynamic chord, m
C_{mL}: Moment derivative with respect to lift
$C_{m\delta_e}$: Moment derivative with respect to control-surface deflection
δ_e: Control-surface deflection, rad
C_{mq}: Moment derivative with respect to pitch rate
ρ: Density of air, kg/m^3
V_{tc}: Equilibrium speed
T_{tc}: Equilibrium thrust
$T_{\max}$: Maximum thrust
θ_{lb}: Lower boundary of pitch angle
$\theta_{\mathrm{balance}}$: Balance pitch angle according to speed scheme
θ_{valid}: Valid pitch angle according to speed scheme
h: Flying height.

Data Availability

The data used to support the findings of this study are available from the corresponding author upon request.

Conflicts of Interest

The authors declare that they have no conflicts of interest regarding the publication of this paper.

Acknowledgments

This research was supported by the Special Funded Project of China Postdoctoral Science Foundation (2019TQ0032) and the Normal Funded Project of China Postdoctoral Science Foundation (2019M660025).

References

[1] T. Jiang, J. Li, B. Li, K. Huang, C. Yang, and Y. Jiang, "Trajectory optimization for a cruising unmanned aerial vehicle attacking a target at back slope while subjected to a wind gradient," *Mathematical Problems in Engineering*, vol. 2015, Article ID 635395, 14 pages, 2015.

[2] R. Hamilton, *Precision Guided Munitions and the New Era of Warfare*, Royal Australian Air Force, Glenbrook, Australia, 2009, https://fas.org/man/dod-101/sys/smart/docs/paper53.htm.

[3] Y. Lappin, *US Army May Soon Use Israeli-Designed "Suicide Drones"*, Jerusalem Post, Jerusalem, Israel, 2016.

[4] R. Martorana, "WASP-a high-G survivable UAV," in *Proceedings of the AIAA's 1st Technical Conference and Workshop on Unmanned Aerospace Vehicles*, Portsmouth, VA, USA, May 2002.

[5] N.-J Bai, X.-F. Fan, and Z.-J Wang, "Research on control algorithms of optimum initiation point of miniature loitering munition," *Journal of Projectiles, Rockets, Missiles and Guidance*, vol. S7, 2006.

[6] G.-L. He, W.-H. Wu, and Z.-H. Li, "Fuzzy control algorithm on a servo controller of loitering munition," *Transactions of Beijing Institute of Technology*, vol. 2, 2009.

[7] J. P. Wilhelm, E. R. Jackson, P. Browning, W. Huebsch, V. Mucino, and M. Gautam, "Flight simulation of a hybrid projectile to estimate the impact of launch angle on range extension," in *Proceedings of the ASME 2012 International Mechanical Engineering Congress and Exposition*, pp. 615–620, Houston, TX, USA, November 2012.

[8] K. Zugel, "Loitering attack munition flight test program," in *Proceedings of the 2nd AIAA "Unmanned Unlimited" Systems, Technologies, and Operations*, San Diego, CA, USA, September 2003.

[9] J. Wilhelm and J. Close, "Roll and pitch produced during an uneven wing deployment of a hybrid projectile," *SAE International Journal of Aerospace*, vol. 7, no. 1, pp. 16–23, 2014.

[10] P. Gnemmi, S. Changey, P. Wey et al., "Flight phases with tests of a projectile-drone hybrid system," *IEEE Transactions on Control Systems Technology*, vol. 26, no. 6, pp. 2091–2105, 2018.

[11] D. Gettinger and A. H. Michel, *Loitering Munitions*, The Center for the Study of the Drone at Bard College, Washington, DC, USA, 2016.

[12] S. Sreeja and H. B. Hablani, "Precision munition guidance and moving-target estimation," *Journal of Guidance, Control, and Dynamics*, vol. 39, no. 9, pp. 2100–2111, 2016.

[13] J. B. Yarwood, M. L. Anderson, L. A. Fumagalli, P. T. Strunk, K. G. Senn, and K. I. Teope, *Novel Munition Design for Low-Collateral Damage Weapons*, AIAA SciTech Forum, San Diego, CA, USA, 2019.

[14] Federation of American Scientists, *AGM-158 Joint Air to Surface Standoff Missile*, Federation of American Scientists, Washington, DC, USA, 2003, https://www.yankee451.com/wp-content/uploads/2012/09/JASSM-Fuse-information.pdf.

[15] G. Frut, "Mistral missile propulsion system," in *Proceedings of the AIAA 25th Joint Propulsion Conference*, Monterey, CA, USA, July 1989.

[16] G. Hu, J. Guo, and J. Zhou, "Integrated guidance and control of interceptors with impact angle constraint against a high-speed maneuvering target," *Proceedings of the Institution of Mechanical Engineers, Part G: Journal of Aerospace Engineering*, vol. 233, no. 14, pp. 5192–5204, 2019.

[17] Q. Hu, T. Han, and M. Xin, "New impact time and angle guidance strategy via virtual target approach," *Journal of Guidance, Control, and Dynamics*, vol. 41, no. 8, pp. 1755–1765, 2018.

[18] S. R. Kumar and T. Shima, "Cooperative nonlinear guidance strategies for aircraft defense," *Journal of Guidance, Control, and Dynamics*, vol. 40, no. 1, pp. 124–138, 2017.

[19] Li Yang, H. Zhou, and W. Chen, "Three-dimensional impact time and angle control guidance based on MPSP," *International Journal of Aerospace Engineering*, vol. 2019, Article ID 5631723, 16 pages, 2019.

[20] P. Lu, "Intercept of nonmoving targets at arbitrary time-varying velocity," *Journal of Guidance, Control, and Dynamics*, vol. 21, no. 1, pp. 176–178, 1998.

[21] Y. Ulybyshev, "Terminal guidance law based on proportional navigation," *Journal of Guidance, Control, and Dynamics*, vol. 28, no. 4, 2005.

[22] P. L. Jimenez, J. A. Silva, and J. S. Hernandez, "Experimental validation of Unmanned Aerial Vehicles to tune PID controllers in open source autopilots," in *Proceedings of the 7th European Conference for Aeronautics and Space Sciences*, Milan, Italy, July 2017.

[23] L. F. Faleiro and A. A. Lambregts, "Analysis and tuning of a "Total Energy Control System" control law using eigenstructure assignment," *Aerospace Science and Technology*, vol. 3, no. 3, pp. 127–140, 1999.

[24] A. L. Smith, "proportional navigation with adaptive terminal guidance for aircraft rendezvous," *Journal of Guidance, Control, and Dynamics*, vol. 31, no. 6, 2008.

[25] J. Wilhelm, J. Close, W. Huebsch, and M. Gautam, "A de-spin and wings-leveling controller for a 40 mm hybrid projectile," *SAE International Journal of Aerospace*, vol. 6, no. 2, pp. 683–692, 2013.

[26] J. Wilhelm, J. Close, and W. Huebsch, "Guidance and range extension control system for a hybrid projectile," in *Proceedings of the SAE 2014 Aerospace Systems and Technology Conference*, Cincinnati, UK, September 2014.

[27] J. M. Maley, "Line of sight rate estimation for guided projectiles with strapdown seekers," in *Proceedings of the AIAA Guidance, Navigation, and Control Conference*, Kissimmee, FA, USA, January 2015.

[28] T. Der-Ren and J.-S. Chern, "A composite guidance strategy for three-dimensional air-to-surface missiles," in *Proceedings of the AIAA Guidance, Navigation, and Control Conference and Exhibit*, pp. 160–174, Boston, MA, USA, August 1998.

[29] J. Zhou, "The existence and uniqueness of the solution for nonlinear elliptic equations in Hilbert spaces," *Journal of Inequalities and Applications*, vol. 2015, no. 1, 2015.

[30] R. M. Brooks and K. Schmitt, "The contraction mapping principle and some applications," *Electronic Journal of Differential Equations*, vol. 9, 2009.

[31] C. A. Mader and J. R. R. A. Martins, "Computing stability derivatives and their gradients for aerodynamic shape optimization," *AIAA Journal*, vol. 52, no. 11, pp. 2533–2546, 2014.

[32] T. Jiang, J. Li, and K. Huang, "Longitudinal parameter identification of a small unmanned aerial vehicle based on modified particle swarm optimization," *Chinese Journal of Aeronautics*, vol. 28, no. 3, pp. 865–873, 2015.

[33] R. M. Cummings, C. M. Liersch, A. Schütte, and K. C. Huber, "Aerodynamics and conceptual design studies on an unmanned combat aerial vehicle configuration," *Journal of Aircraft*, vol. 55, no. 2, 2018.

[34] W. P. VanSkike, M. A. Williams, T. Stastny, A. Ghate, S. E. McCandless, and T. J. Peckman, "Hawkeye UAV dynamic analysis," in *Proceedings of the AIAA Modeling and Simulation Technologies Conference*, Portland, ORE, USA, August 2011.

[35] G. Ciraolo and L. Vezzoni, "On Serrin's overdetermined problem in space forms," *Manuscripta Mathematica*, vol. 159, no. 3-4, pp. 445–452, 2019.

[36] A. A. Abramov and L. F. Yukhno, "The least square method for systems of linear ordinary differential equations," *Computational Mathematics and Mathematical Physics*, vol. 59, no. 6, pp. 915–925, 2019.